NANO LETTERS

Letter

pubs.acs.org/NanoLett

Two-Dimensional Heterostructure as a Platform for Surface-Enhanced Raman Scattering

Yang Tan,*[,†] Linan Ma,[†] Zhibin Gao,[‡,§,⊥] Ming Chen,[†] and Feng Chen*[,†]

[†]School of Physics, State Key Laboratory of Crystal Materials, Shandong University, Shandong, Jinan 250100, P. R. China

[‡]Center for Phononics and Thermal Energy Science, School of Physics Science and Engineering, Tongji University, 200092 Shanghai, P. R. China

[§]China-EU Joint Center for Nanophononics, School of Physics Science and Engineering, Tongji University, 200092 Shanghai, P. R. China

[⊥]Shanghai Key Laboratory of Special Artificial Microstructure Materials and Technology, School of Physics Science and Engineering, Tongji University, 200092 Shanghai, P. R. China

Supporting Information

ABSTRACT: Raman enhancement on a flat nonmetallic surface has attracted increasing attention, ever since the discovery of graphene enhanced Raman scattering. Recently, diverse two-dimensional layered materials have been applied as a flat surface for the Raman enhancement, attributed to different mechanisms. Looking beyond these isolated materials, atomic layers can be reassembled to design a heterostructure stacked layer by layer with an arbitrary chosen sequence, which allows the flow of charge carriers between neighboring layers and offers novel functionalities. Here, we demonstrate the heterostructure as a novel Raman enhancement platform. The WSe_2 (W) monolayer and graphene (G) were stacked together to form a heterostructure with an area of 10 mm × 10 mm. Heterostructures with different stacked structuress are used as platforms for the enhanced Raman scattering, including G/W, W/G, G/W/G/W, and W/G/G/W. On the surface of the heterostructure, the intensity of the Raman scattering is much stronger compared with isolated layers, using the copper phthalocyanine (CuPc) molecule as a probe. It is found that the Raman enhancement effect on heterostructures depends on stacked methods. Phonon modes of CuPc have the strongest enhancement on G/W. W/G and W/G/G/W have a stronger enhancement than that on the isolated WSe_2 monolayer, while lower than the graphene monolayer. The G/W/G/W/substrate demonstrated a comparable Raman enhancement effect than the G/W/substrate. These differences are due to the different interlayer couplings in heterostructures related to electron transition probability rates, which are further proved by first-principle calculations and probe−pump measurements.

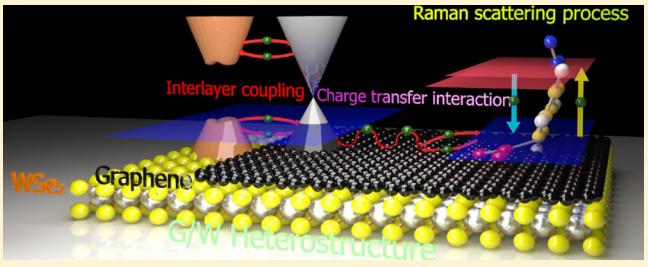

KEYWORDS: *Heterostructure, surface-enhanced Raman scattering*

The Raman enhancement effect has attracted continuous attention in both applied and academic research, due to its significant values for microanalytical applications and fundamental studies of light−matter (or matter−matter) interaction.[1] As a type of Raman enhancement technique, surface-enhanced Raman scattering (SERS) enables the detection of a single molecule via the excitation of the rough substrate or nanostructures.[2−6] Although SERS is intensively studied, there are still many controversies regarding the pertinent enhancement mechanism. Until now, two mechanisms have been widely accepted for the SERS, the so-called electromagnetic mechanism (EM)[6] and chemical mechanism (CM).[6] (1) EM depends on the enhancement of the local electromagnetic fields (surface plasmon excited by the incident light) around the metallic structures, which is clearly explained in both theoretical and experimental researches. (2) CM is induced by the charge transfer between the substrate and the molecule, which is not well-understood. Compared with CM, the EM effect needs noble metals as the substrate for SERS, which has several disadvantages, including extra adsorbates on the surface due to the catalytic effect and the strong spectral background.[7−11] Nonmetallic materials with the CM effect are considered as an excellent candidate substrate for SERS to overcome these disadvantages. Meanwhile, the booming development of the two-dimensional material also provides diverse platforms for the studying of CM effect on nonmetal materials. Since 2010, diverse 2D materials have been reported as Raman enhancement substrates such as graphene, Si or Ge nanostructures, hexagonal boron nitride (h-BN), and molybde-

Received: January 30, 2017
Revised: March 28, 2017
Published: March 29, 2017

DOI: 10.1021/acs.nanolett.7b00412
Nano Lett. 2017, 17, 2621−2626

num disulfide (MoS_2), which have different enhancement mechanisms.[12]

Due to differences in the mechanisms, diverse 2D materials have their own merits and demerits. For instance, the graphene depends on the ground-state charge transfer at the interface, while the enhancement of the Raman scattering is limited by the electronic state density of graphene.[13,14] The transition metal dichalcogenides (TMD) with three atomic layers has a more complex band structure and abundant electronic states. But, the intensity of the Raman scattering is weak due to the cooperation of both the ground-state charge transfer and the dipole−dipole coupling.[12] The heterostructure provides a potential solution for the mutual complementarity of different 2D materials.[15,16]

The heterostructure is assembled by stacking different 2D crystals on the top of each other.[17] Layered 2D materials are held together via the van der Waals force, allowing the interlayer electronic tunneling.[18] Designing the sequence of stacked layers, the electronic band structure can be artificially built, offering 2D heterostructure unique chemical or physical functionalities, including enhanced saturable absorption,[19] ultrafast photoresponse,[20] and photoluminescence.[21] As the CM effect strongly relies on the electronic structure of the substrate, it could be predicted that the heterostructure with artificially designed sequence can bring in new phenomenon for the SERS.

In this work, we demonstrate the graphene-based heterostructure as an efficient platform for SERS. CuPc is used as the probe molecule, due to its strong Raman scattering. The heterostructure was constructed by the monolayer graphene and WSe_2 (tungsten-based dichalcogenide) with an artificial sequence. Compared with the monolayer platform, the heterostructure was proved to have stronger SRES. As the interlayer coupling in the heterostructure increases the electronic state density of the 2D material on the surface, it meanwhile increases the electronic transition probability at the contact surface of the CuPc molecule and consequently enhances the CM effect of the heterostructure. Our work proposes the heterostructure as a novel platform for both study and application of the CM effect of SERS.

We produced graphene and WSe_2 monolayers with dimensions of 10 mm × 10 mm by chemical vapor deposition on the copper and aluminum oxide (Al_2O_3) wafers, separately. The heterostructure was built by the wet-chemical transfer technique via putting graphene and the WSe_2 monolayer on the top of each other. As monolayers (graphene and WSe_2) were mechanically stacked together on the Al_2O_3 wafer, there are ripples and corrugations on the transferred monolayer, and layers are not tightly attached with each other. The measured interlayer distance of the as-prepared heterostructure is ~4 nm. To compact the as-prepared heterostructure, each sample used in this work was irradiated by the carbon ion beam with the energy of 6 MeV and the fluence of 1×10^{13} ions/cm^2. The ion beam irradiation has recently been proved to be an efficient technique to tailor the properties of 2D materials for diverse purposes (see Part I in Supporting Information, SI).

Figure 1a shows the atomic force microscope (AFM) topographic data of the heterostructure with the graphene on the top of WSe_2 (G/W). The measured thicknesses of the G/W heterostructure and WSe_2 were 1.4 and 0.7 nm, indicating the interlayer distance of 0.4 nm referred to the monolayer thickness of graphene (0.3 nm). The Raman spectrum of the heterostructure was used to characterize the quality of the

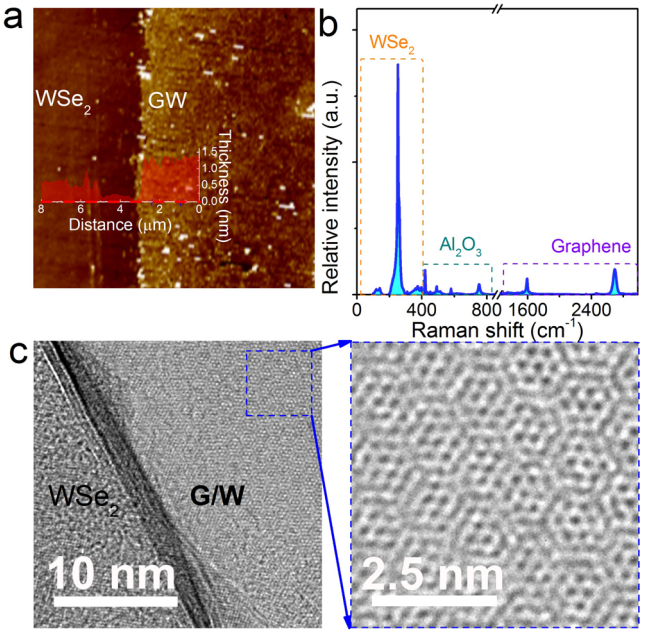

Figure 1. (a) AFM topographic image of the heterostructure with graphene on the top of WSe_2 (G/W). The inset is the thickness along the red dashed line. (b) Raman spectrum of the G/W heterostructure. (c) HRTEM image of a boundary region of the WSe_2 monolayer and the G/W heterostructure, showing the Moiré pattern.

stacked layers within the range of 100−400 nm (WSe_2) and 1000−3000 nm (graphene). As displayed in Figure 1b, the WSe_2 monolayer has the bandwidth (W) of 7.7 cm^{-1} and the position of the Raman peak at 252.6 nm, accordance with the intrinsic structure of WSe_2.[22] For graphene, the intensity ratio of G and 2D peaks is 0.4 (I_G/I_{2D}), demonstrating the monolayer of graphene.[23,24] Besides, the tiny intensity ratio of D and G peaks indicates the low density of the zero-dimensional point-like defects in graphene. These measurements prove that the intrinsic structures of graphene and WSe_2 are well-preserved after the wet-chemical transfer and the carbon ion irradiation. Figure 1c displays the high-resolution transmission electron microscopy (HRTEM) image of G/W heterostructure at the boundary region between monolayer WSe_2 and G/W bilayer. As the WSe_2 and graphene have the lattice mismatching, the heterostructure lattice forms a Moiré pattern.

CuPc molecules were deposited onto the Al_2O_3 substrate, G/W heterostructure, WSe_2 (W) monolayer, and graphene (G) monolayer, respectively, by the Langmuir−Blodgett (LB) technique (Figure 2a). The characterization of the CuPc LB film is shown in Part II of the SI. Figure 2b shows the comparison of the Ramen scattering of the CuPc LB film, using the 632.8 nm laser as the excitation light with the power of 8 mW and exposure time of 2 s. On platforms of G, W, and G/W, SERS of the CuPc molecule was observed. Their enhancement factors were calculated by comparing their Raman intensity with the one on the Al_2O_3 substrate. For 1528.3 cm^{-1} mode, the enhancement factor of G, W, and G/W are 4.7, 9.9, and 28.6, respectively. Obviously, the G/W has the largest enhancement factor, even larger than the sum of G and W. Figure 2c shows the Raman mapping at the peak of 1528.3 cm^{-1}, with the 632 nm laser as the excitation light. We further confirmed this enhancement phenomenon on these substrates

DOI: 10.1021/acs.nanolett.7b00412
Nano Lett. 2017, 17, 2621−2626

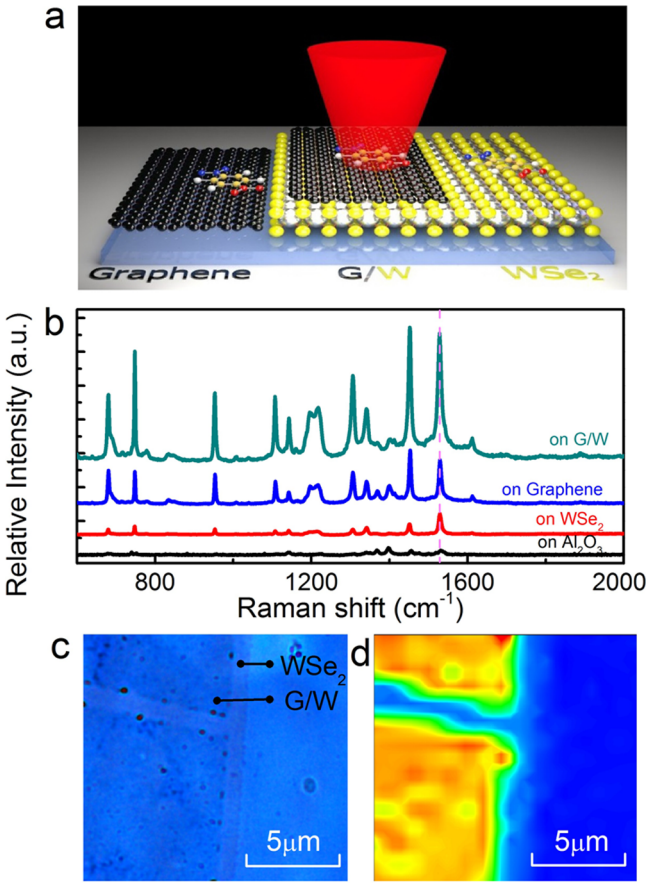

Figure 2. (a) Schematic illustration of the measurement procedure and prepared samples including graphene, WSe_2, and G/W heterostructure. (b) Raman spectra of the CuPc molecule on the substrates of the Al_2O_3 wafer (black solid line), WSe_2 (red solid line), graphene (blue solid line), and G/W (cyan solid line). (c) The optical image of G/W and the Raman mapping image for the CuPc molecule at 1528.3 cm^{-1}.

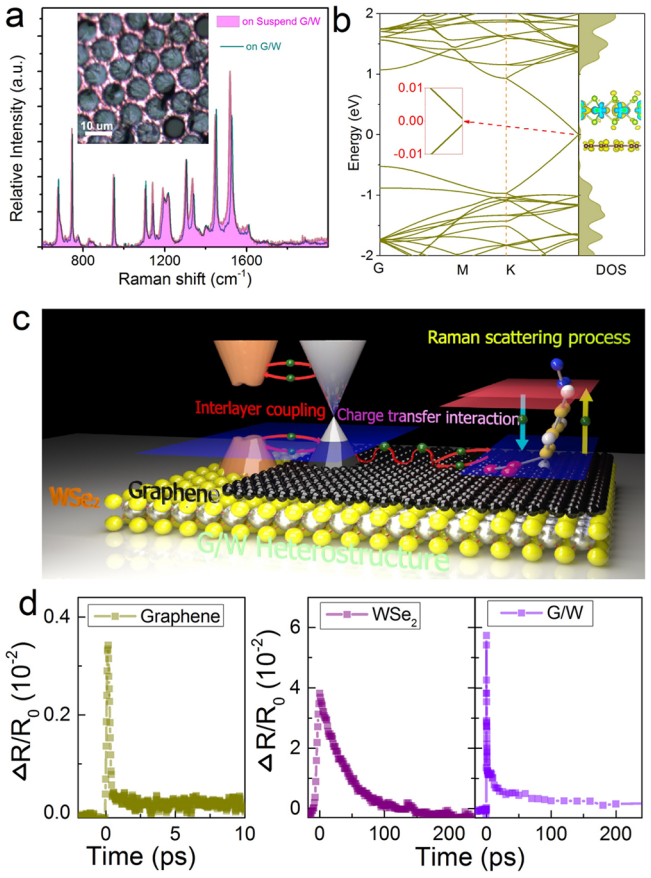

Figure 3. (a) Raman spectra of the CuPc molecule on the G/W (cyan solid line) and suspended G/W (magenta solid line). The inset is the microscope graph of the suspended G/W. (b) Electronic band structure and DOS of G/W. The inset is the charge density difference isosurface. (c) Schematic diagram showing electronic transitions in the G/W heterostructure. (d) The measured time-resolved differential reflection of the probe pulse from graphene, WSe_2, and G/W.

by using the 4ATP as a probe and the 632.8 nm laser as the excitation light (see Part III in the SI).

To exclude the influence from the Al_2O_3 substrate, we carried out the same experiments on the suspend G/W. The suspension sample was fabricated by transferring graphene and WSe_2 monolayer onto the surface of a transmission electron microscopy (TEM) grid. Figure 3a displayed a comparison of the Raman spectra of the CuPc from the G/W with the Al_2O_3 substrate and the suspended G/W, respectively. The enhancement is similar to each other, demonstrating that the enhancement effect is an intrinsic property of 2D materials. Table 1 lists all intensity peaks of the CuPc Raman modes on different substrates. Raman upshifts (679.5, 739.8, 1140.4, 1172.6, 1340.9, and 1367.9 cm^{-1}) and downshifts (1109.2, 1310.6, 1456.2, and 1531.5 cm^{-1}) were observed on 2D materials relative to the one on Al_2O_3 substrate. It indicates there is a tight contact of CuPc molecule with 2D materials, where a vibrational coupling occurs between the molecule and 2D materials. Besides, all vibrational modes of CuPc have an enhancement with different enhancement factors, which vary over a wide range from 1.6 to 78.2 due to different chemical enhancement effects. The CuPc molecule has the largest enhancement for the 1107 cm^{-1} mode, which is about 78.2 times on G/W and 27.7 (4.2) times on G (W). In the following, we will explore the mechanism for this enhanced SRES on G/W, through the comparison of the mechanisms for graphene and WSe_2.

The Raman scattering enhancements of the graphene and WSe_2 monolayers are explained by the enhanced charge transfer (CM effect of the SERS) between the 2D material and CuPc molecules.[12] The electron transition probability rate between materials can be expressed as below, according to Fermi's golden rule:

$$w_{lk} = \frac{2\pi}{\hbar} g(E_k)|H'_{kl}|^2 \quad (1)$$

where the $g(E_k)$ is the density of states and H'_{kl} is the matrix element for the LUMO−HOMO transition. As graphene has a zero-band gap, there are numerical electron states around the HOMO (highest-occupied molecular orbital) and the LUMO (lowest-unoccupied molecular orbital) levels of the CuPc molecule. The contact of the molecule and graphene will increase the electronic density of states ($g(E_k)$) and consequently increase the electron transition probability rate according to eq 1. On the interface of the CuPc molecule and WSe_2, there are both interface dipole interactions (due to the W−Se bond) and the electronic transition. The dipole interaction can result in a local symmetryrlated perturbation, which increases the matrix element H'_{kl}. However, both the electronic transition and the dipole interaction are weak, as the

DOI: 10.1021/acs.nanolett.7b00412
Nano Lett. 2017, 17, 2621−2626

Table 1. Enhancement Factor of CuPc Raman Modes on Different Substrates

ω_{sub} (cm^{-1})	ω_W (cm^{-1})	ω_G (cm^{-1})	$\omega_{G/W/Al2O3}$ (cm^{-1})	EF_W	EF_G	$EF_{G/W/Al2O3}$	mode assignment
679.5	679.5	680.7	680.7	3.9	26.4	51.4	B_{1g}, in plane full symmetric nonmetal bound N−M stretch and outer ring
739.8	748.1	748.1	748.1	3.3	12.9	43.6	stretches
1109.2	1107.0	1108.1	1107.0	4.2	27.7	78.2	A_{1g}, in plane full symmetric N−M stretch
1140.4	1141.5	1142	1142.6	1.6	5.5	20.0	A_{1g}, in plane symmetric N−M−N bend
1172.6	1198.0	1196.9	1195.8	2.7	18.5	49.7	B_{2g}, in plane ring symmetric and outer rings breathing
1310.6	1306.3	1306.3	1306.3	4.7	29.1	77.6	A_{2g}
1340.9	1342.0	1340.9	1340.9	3.0	10.1	23	B_{2g}
1367.9	1367.9	1369	1368.9	0.18	2.8	3.8	B_{2g}, in plane symmetric outer ring rotation
1456.2	1450.8	1453	1451.9	2.5	13.2	32.4	B_{1g}, in plane full symmetric N−C stretch and ring C−C stretch
1531.5	1529.4	1528.3	1528.3	4.7	9.9	28.6	B_{2g}, in plane ring symmetric outer ring C−C stretch

[a] ω is the Raman shift of the CuPc molecule on the Al_2O_3 substrate, W/Al_2O_3, G/Al_2O_3, and $G/W/Al_2O_3$, respectively. $EF_{Substrate}$ is the intensity ratio of Raman signals on different substrates.

WSe_2 is a semiconductor and a weak polar material (as WSe_2 has three atomic layers with tungsten atoms in the center layer and selenium atoms on the outside layers). Therefore, the observed surface-enhanced Raman scattering is weak on the WSe_2 monolayer.

On the G/W, the CuPc molecule has the same surface interaction compared with graphene. However, the electronic state density of graphene is changed by the WSe_2 monolayer through the interlayer coupling. To demonstrate the variation of the electronic state density, we calculated the electronic structure of G/W by the density function theory (DFT) via the Vienna ab initio simulation package known as the VASP code,[25−27] and the electronic−ion interaction was described by the projector augmented wave method (PAW).[28,29]

The equilibrium distance between graphene and WSe_2 is determined to be 0.3 nm, which is close to the one measured in Figure 1a, indicating the optimized combination of graphene and the WSe_2 monolayer after the carbon ion irradiation. The calculated electronic band structure and projected density of states (PDOS) of this heterostructure are shown in Figure 3b, in which WSe_2 is insulated by graphene, and their electronic structure is similar to the overlapping of isolated monolayers. However, there are two aspects should be noticed. (1) G/W heterostructure has wave functions located in both graphene and WSe_2, allowing the electronic tunneling between neighbored layers (inset in Figure 3b). As a result, the electronic state density of graphene is increased due to the coupling with WSe_2 and finally increases the electronic density of states ($g(E_k)$) on the interface of the molecule and graphene. (2) At the K point, the interaction between graphene and WSe_2 opens a tiny gap, tuning the graphene to a semiconducting with a direct gap. But this narrow fundamental gap is too small to affect the energy matching between energy levels of CuPc molecules and the Fermi level of graphene, indicating a little negative influence on the charge transfer. Therefore, the enhancement factor on the surface of G/W heterostructure is intrigued by the enriched electronic state density, due to the interlayer coupling in the heterostructure. Figure 3c shows the schematic diagram of electronic transitions in the G/W heterostructure.

The above analysis is further supported by the probe−pump measurement, which can present the charge transfer at van der Waals interfaces. During the measurement, the differential reflection induced by the photoexcited carriers was monitored via the time-resolved differential reflection ($\Delta R/R_0$) of the probe pulse by a mode-locked Yb:KGW based fiber laser (190 fs, 512 nm, 20 Hz) with the same setup in ref 29. Under the same conditions, differential reflections of graphene, WSe_2, and G/W are measured (Figure 3d). In the individual monolayer, the magnitude of the peak signal of graphene (0.34×10^{-2}) was almost one tenth of the WSe_2 (3.8×10^{-2}). Meanwhile, in G/W, the magnitude is 1.4 times higher than the sum of individuals, and the single-exponential decay time is 5 ps, which is close to graphene (5 ps) and much shorter than WSe_2 (150 ps). These observations imply there is the interlayer coupling between the graphene and WSe_2. In respect to the isolated graphene/WSe_2, the heterostructure exhibits a stronger electronic density states and faster charge transfer effect.

The function of the heterostructure depends on the stacking types of 2D materials, including the number and the sequence of layers. In the following, we discuss the influence of the stacked way to the Raman enhancement. In Figure 4a, the

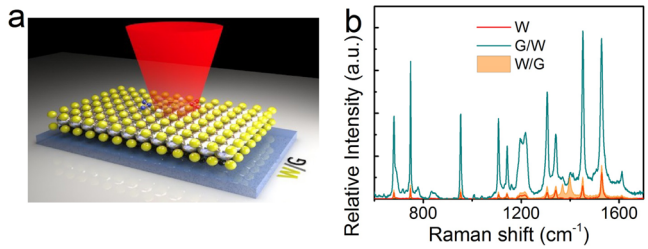

Figure 4. (a) Schematic illustration of the measurement procedure. (b) Raman spectrum of the CuPc molecule on the substrate of W/G (orange solid line). Raman spectra from G/W (cyan, yellow dashed lines) and WSe_2 (red dotted line) are shown as references.

WSe_2 monolayer was put on the top of graphene (W/G), and the CuPc was added on the surface of the WSe_2 monolayer. The Raman spectrum from W/G is much lower than the one on G/W heterostructure and slightly higher than the WSe_2 monolayer (Figure 4b). G/W and W/G have the same composition, except for the interface with the CuPc molecule. We believe that the difference of SERS is induced by the layered material at the interface. For the WSe_2 monolayer, both the electronic transition and the dipole interaction are low, leading to a weak SERS. The graphene on the bottom may increase the electronic transition of the WSe_2 and enhances the SERS on the surface of WSe_2. But the increase of the electronic transition is limited by the efficiency of the interlayer coupling and is not stronger than the graphene itself. As the result, the SERS from W/G is lower than the graphene monolayer.

DOI: 10.1021/acs.nanolett.7b00412
Nano Lett. 2017, 17, 2621−2626

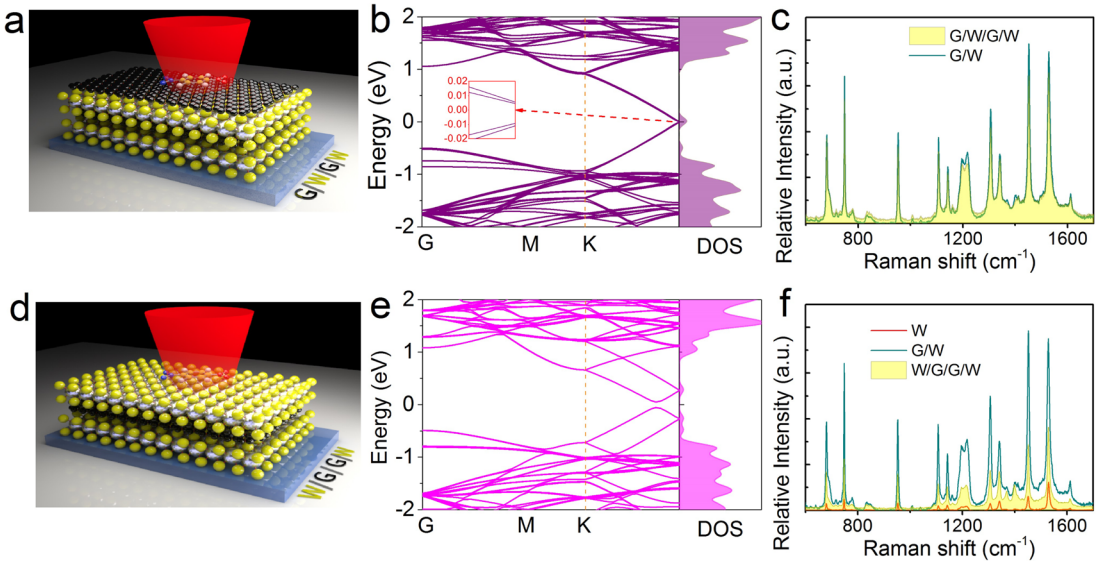

Figure 5. Panels a and d are the schematic illustration of the measurement procedure. Raman spectra of the CuPc molecule on the substrate of (b) G/W/G/W (green solid line) and (e) W/G/G/W (orange solid line). Electronic band structure and DOS of (c) G/W/G/W (purple solid line) and (f) W/G/G/W (magenta solid line). Raman spectra from G/W (cyan solid line) and WSe_2 (red solid line) are shown as references.

Figure 5a shows the interval stacked four-layer heterostructure (G/W/G/W) with graphene on the top. In this configuration, the electronic structure is similar to G/W, in which the linear dispersion bands of graphene has a tiny gap at the K point and coupling states are discovered between layers (Figure 5b). However, the Raman scattering of the CuPc molecule from G/W/G/W is similar to the one on G/W (Figure 5c). We speculate that the charge transfer between interval layers is much weaker than the neighbor layers and the Raman enhancement is hardly affected by the charge transfer from 2D materials far away from the surface.

Figure 5d shows a heterostructure stacked to a sandwich structure with two graphene layers in the center and WSe_2 layers on the outside (W/G/G/W). The electronic structure of W/G/G/W has a bigger direct bandgap between K and M points compared with W/G, resulting in a lower Fermi level in W/G/G/W (Figure 5e). Meanwhile, the electron density of W/G/G/W is larger than W/G, increasing the electron transition probability rate and enhancing Raman scattering. As shown in Figure 5f, the Raman enhancement is stronger on W/G/G/W than the one on W/G.

Several trends can be summarized based on previous experimental results. (1) Interlayer interactions in the heterostructure enhance the Raman scattering on the surface via increasing the charge transfer at the interface. The magnitude of the enhancement fact depends on the 2D material on the top. (2) The Raman enhancement of the heterostructure is a surface effect. The heterostructure with more than two layers has a little impact on the enhancement of the charge transfer, resulting in the similar performance of the Raman enhancement with the bilayer heterostructure.

In this work, we propose the graphene based heterostructure as a novel platform for the surface Raman enhancement. Via carbon ion irradiation, the interlayer distance of the heterostructure was decreased from ~4 nm to ~0.4 nm to reach the optimized combination of graphene and the WSe_2 monolayer. The interlayer coupling between layers enhances the Raman scattering of the CuPc molecule on the surface of the heterostructure. Furthermore, we discussed the influence of the stacking sequence to the Raman enhancement. It was found that the SERS intensity is a surface effect, whereas the enhancement factors are close with the heterostructure more than two layers. The reason for these phenomena was explained by the first-principles calculation and the probe–pump measurement. This work proposes a new avenue to enhance the Raman scattering of the molecule and provides a new platform for the analysis of the CM effect.

Methods. *Sample Preparation.* We produced graphene and WSe_2 monolayers by the chemical vapor deposition (CVD) on copper and Al_2O_3 wafers with dimensions of 10 mm × 10 mm, respectively. Through the wet-chemistry transfer process, graphene and WSe_2 were stacked together on the substrate of Al_2O_3 constituting a heterostructure. Then the heterostructure was irradiated by 6 MeV carbon (C^{3+}) ions at a fluence of 1×10^{13} ions/cm^2 by a 2 × 1.7 MV tandem accelerator at Peking University.

Probe–Pump Measurement. We perform probe–pump measurements with a mode locked Yb:KGW based fiber laser (190 fs, 515 nm, 20 Hz). The pulse laser was divided into the pumping and probe beams via a beam splitter. Through a system of half plate and polarizor, the peak power of the probe light is set to 8% of the pumping light, to avoid the nonlinear effect induced by the probe beam. The measurements of the probe and pumping light are 22 mm and 152 mm, respectively. A variable delay was put into the pump path, and the variation of the probe light intensity versus the delay time by an energy detector was recorded after the pumping light.

DFT Calculations. The electron–ion interaction is described by a projector augmented wave method (PAW). The energy cutoff of the plane waves is set to 450 eV with an energy precision of 10^{-5} eV. The electron exchange–correlation function is treated using a generalized gradient approximation (GGA) in the form proposed by Perdew, Burke, and Ernzerhof (PBE). The Monkhorst–Pack *k*-point meshes for the Brillouin zone (BZ) sampling used in structural optimization and electronic structure calculations are 3 × 3 × 1 and 5 × 5 × 1, respectively. A vacuum region up to 15 Å is applied to exclude the interaction between adjacent images. Both atomic

DOI: 10.1021/acs.nanolett.7b00412
Nano Lett. 2017, 17, 2621–2626

positions are fully optimized using the conjugate gradient (CG) algorithm until the maximum atomic forces are less than 0.001 eV/Å.

■ ASSOCIATED CONTENT

Supporting Information

The Supporting Information is available free of charge on the ACS Publications website at DOI: 10.1021/acs.nanolett.7b00412.

Sample preparation, ion irradiation, assembly of CuPc LB film, Raman enhancement of 4ATP, intensity comparison of CuPc Raman modes on different platforms, and the UV−vis absorption spectrum of the CuPc LB film (PDF)

■ AUTHOR INFORMATION

Corresponding Authors

*E-mail: tanyang@sdu.edu.cn.
*E-mail: drfchen@sdu.edu.cn.

ORCID

Yang Tan: 0000-0001-7912-1742
Zhibin Gao: 0000-0002-6843-381X
Feng Chen: 0000-0002-9277-9810

Notes

The authors declare no competing financial interest.

■ ACKNOWLEDGMENTS

This work is supported by the National Natural Science Foundation of China (no. 11535008) and 111 Project of China (B13029). Y.T. acknowledges the financial support from Young Scholars Program of Shandong University (no. 2015WLJH20).

■ REFERENCES

(1) Rygula, A.; Majzner, K.; Marzec, K. M.; Kaczor, A.; Pilarczyk, M.; Baranska, M. *J. Raman Spectrosc.* **2013**, *44*, 1061−1076.
(2) Schatz, G. C.; Young, M. A.; Duyne, R. P. V. In Surface-Enhanced Raman Scattering. Kneipp, K., Moskovits, M., Kneipp, H., Eds.; *Topics in Applied Physics*; Springer: Berlin, 2006; pp 19−45.
(3) Wu, D.-Y.; Liu, X.-M.; Duan, S.; Xu, X.; Ren, B.; Lin, S.-H.; Tian, Z.-Q. *J. Phys. Chem. C* **2008**, *112*, 4195−4204.
(4) Yamada, H.; Nagata, H.; Toba, K.; Nakao, Y. *Surf. Sci.* **1987**, *182*, 269−286.
(5) Maitani, M. M.; Ohlberg, D. A. A.; Li, Z.; Allara, D. L.; Stewart, D. R.; Williams, R. S. *J. Am. Chem. Soc.* **2009**, *131*, 6310−6311.
(6) Otto, A. *J. Raman Spectrosc.* **2005**, *36*, 497−509.
(7) Campion, A.; Kambhampati, P. *Chem. Soc. Rev.* **1998**, *27*, 241−250.
(8) Xu, W.; Ling, X.; Xiao, J.; Dresselhaus, M. S.; Kong, J.; Xu, H.; Liu, Z.; Zhang, J. *Proc. Natl. Acad. Sci. U. S. A.* **2012**, *109*, 9281−9286.
(9) Hurst, S. J.; Fry, H. C.; Gosztola, D. J.; Rajh, T. *J. Phys. Chem. C* **2011**, *115*, 620−630.
(10) Musumeci, A.; Gosztola, D.; Schiller, T.; Dimitrijevic, N. M.; Mujica, V.; Martin, D.; Rajh, T. *J. Am. Chem. Soc.* **2009**, *131*, 6040−6041.
(11) Sun, Z.; Wang, C.; Yang, J.; Zhao, B.; Lombardi, J. R. *J. Phys. Chem. C* **2008**, *112*, 6093−6098.
(12) Ling, X.; Fang, W.; Lee, Y.; Araujo, P. T.; Zhang, X.; Rodriguez-Nieva, J. F.; Lin, Y.; Zhang, J.; Kong, J.; Dresselhaus, M. S. *Nano Lett.* **2014**, *14*, 3033−3040.
(13) Ling, X.; Xie, L. M.; Fang, Y.; Xu, H.; Zhang, H. L.; Kong, J.; Dresselhaus, M. S.; Zhang, J.; Liu, Z. F. *Nano Lett.* **2010**, *10*, 553−561.
(14) Qiu, C. Y.; Zhou, H. Q.; Yang, H. C.; Chen, M. J.; Guo, Y. J.; Sun, L. F. *J. Phys. Chem. C* **2011**, *115*, 10019−10025.
(15) Zeng, S.; Hu, S.; Xia, J.; Anderson, T.; Dinh, X.; Meng, X.; Coquet, P.; Yong, K. *Sens. Actuators, B* **2015**, *207*, 801−810.
(16) Mishra, A. K.; Mishra, S. K.; Verma, R. K. *J. Phys. Chem. C* **2016**, *120*, 2893−2900.
(17) Peimyoo, N.; Yu, T.; Shang, J. Z.; Cong, C. X.; Yang, H. P. *Carbon* **2012**, *50*, 201−208.
(18) Georgiou, T.; Jalil, R.; Belle, B. D.; Britnell, L.; Gorbachev, R. V.; Morozov, S. V.; Kim, Y.; Gholinia, A.; Haigh, S. J.; Makarovsky, O.; Eaves, L.; Ponomarenko, L. A.; Geim, A. K.; Novoselov, K. S.; Mishchenko, A. *Nat. Nanotechnol.* **2012**, *8*, 100.
(19) Mu, H.; Wang, Z.; Yuan, J.; Xiao, S.; Chen, C.; Chen, Y.; Chen, Y.; Song, J.; Wang, Y.; Xue, Y.; Zhang, H.; Bao, Q. *ACS Photonics* **2015**, *2*, 832.
(20) Lee, C.; Lee, G.; van der Zande, A. M.; Chen, W.; Li, Y.; Han, M.; Cui, X.; Arefe, G.; Nuckolls, C.; Heinz, T. F.; Guo, J.; Hone, J.; Kim, P. *Nat. Nanotechnol.* **2014**, *9*, 676.
(21) Eftekhari, E.; Li, X.; Kim, T. H.; Gan, Z.; Cole, I. S.; Zhao, D.; Kielpinski, D.; Gu, M.; Li, Q. *Sci. Rep.* **2015**, *5*, 14439.
(22) Sahin, H.; Tongay, S.; Horzum, S.; Fan, W.; Zhou, J.; Li, J.; Wu, J.; Peeters, F. M. *Phys. Rev. B: Condens. Matter Mater. Phys.* **2013**, *87* (16), 165409.
(23) Kim, J.; Hwang, J. H.; Suh, J.; Tongay, S.; Kwon, S.; Hwang, C. C.; Wu, J.; Park, J. Y. *Appl. Phys. Lett.* **2013**, *103*, 171604.
(24) Huang, Y.; Wu, J.; Hwang, K. C. *Phys. Rev. B: Condens. Matter Mater. Phys.* **2006**, *74*, 245413.
(25) Hashimoto, A.; Suenaga, K.; Gloter, A.; Urita, K.; Iijima, S. *Nature* **2004**, *430*, 870.
(26) Sahin, H.; Tongay, S.; Horzum, S.; Fan, W.; Zhou, J.; Li, J.; Wu, J.; Peeters, F. M. *Phys. Rev. B: Condens. Matter Mater. Phys.* **2013**, *87* (16), 165409.
(27) Huang, Y.; Wu, J.; Hwang, K. C. *Phys. Rev. B: Condens. Matter Mater. Phys.* **2006**, *74*, 245413.
(28) Zhao, W.; Ghorannevis, Z.; Chu, L.; Toh, M.; Kloc, C.; Tan, P.; Eda, G. *ACS Nano* **2013**, *7*, 791.
(29) Xia, T.; Dogariu, A.; Mansour, K.; Hagan, D. J.; Said, A. A.; Van Stryland, E. W.; Shi, S. *J. Opt. Soc. Am. B* **1998**, *15*, 1497.

DOI: 10.1021/acs.nanolett.7b00412
Nano Lett. 2017, 17, 2621−2626